MAPPING FOREST LEAF AREA INDEX USING REFLECTANCE AND TEXTURAL INFORMATION DERIVED FROM WORLDVIEW-2 IMAGERY IN A MIXED NATURAL FOREST AREA IN FLORIDA, USA

Ruiliang Pu and Jun Cheng
School of Geosciences
University of South Florida
4202 E. Fowler Avenue, NES 107
Tampa, FL 33620 USA
Email: rpu@usf.edu
Email: jun@mail.usf.edu

ABSTRACT

The leaf area index (LAI) of plant canopies is an important structural parameter that controls energy, water, and gas exchanges of plant ecosystems. Remote sensing techniques may offer an alternative for measuring and mapping forest LAI at a landscape scale. Given the characteristics of high spatial / spectral resolution of the WorldView-2 (WV2) sensor, it is of significance that the textural information extracted from WV2 multispectral (MS) bands will be first time used in estimating and mapping forest LAI. In this case, LAI mapping accuracies would be compared from (a) spatial resolutions between 2-m WV2 MS data and 30-m Landsat TM imagery, (b) the nature of variables between spectrum-based features and texture-based features, and (c) sensors between TM and WV2. In this study, spectral/spatial features (SFs) were selected and tested, including band reflectance, various vegetation indices and 1st and 2nd-order statistical texture measures; a canonical correlation analysis was performed with different data sets of SFs and LAI measurement; and finally linear regression models were used to predict and map forest LAI with canonical variables calculated from image data. The experimental results demonstrate that for estimating and mapping forest LAI, (i) using high resolution data is better than using relatively low resolution data; (ii) extracted from the same WV2 data, texture-based features have higher capability than that of spectrum-based features; (iii) a combination of spectrum-based features with texture-based features could lead to even higher accuracy of mapping forest LAI than their either one separately; and (iv) WV2 sensor outperforms TM sensor significantly. In addition, the experimental results also indicate that the Red-edge band in WV2 has performed the worst on estimating LAI, compared to other WV2 MS bands and the WV2 MS bands in the visible range have a much higher correlation with ground measured LAI than that of Red-edge and NIR bands.

INTRODUCTION

The leaf area index (LAI) of plant canopy is an important structural parameter that controls energy, water, and gas exchanges of plant ecosystems, such as photosynthesis, respiration, transpiration, carbon and nutrient cycle, and rainfall interception (e.g., Running et al., 1989; Gong et al., 1995; White et al., 1997; Chen et al., 2002; Schlerf et al., 2005). Therefore, accurate mapping of LAI spatial distribution is critical for better understanding of the structures and functions of plant ecosystems and for quantitative analysis of many physical and biological processes (Chen et al., 2002). Nevertheless, ground-based measurement of canopy LAI is labor-intensive and, thus, is problematic over large areas (Gobron et al., 1997). Remote sensing techniques, especially high resolution satellite remote sensing, may offer an alternative for measuring and mapping LAI at a landscape scale or even a regional scale.

During the last two decades, many studies have demonstrated the potential of high resolution satellite remote sensing sensors (such as IKONOS, QuickBird and WorldView-2 (WV2)) for estimating and mapping forest LAI spatially and temporally (e.g., Colombo et al., 2003; Soudani et al., 2006; Song and Dickinson, 2008; Gray and Song, 2012; Gu et al., 2012; Zhou et al., 2014). Due to the high spatial resolution of these satellite sensors' data, frequently used spatial information derived from these high resolution images, called texture-based features or texture measures, could be used to effectively predict and map plant LAI. For examples, Colombo et al. (2003) used both vegetation indices (VIs) and texture measures derived from IKONOS image data to retrieve the LAI of different vegetation types and concluded that the combination of the texture measures and VIs results in an

improved fit in a regression equation for most vegetation types when compared with spectral VIs only. In extracting conifer- and hardwood-dominated forest canopy structural parameters, including forest LAI from spatial information of high resolution IKONOS imagery, Song and Dickinson (2008) demonstrated that image spatial information is more useful in estimating LAI than two VIs (NDVI and simple ratio VI) and combining both spatial and spectral information provides some improvement in estimating LAI compared with using spectral information only. With spatial information derived from QuickBird imagery, Zhou et al. (2014) evaluated three different image processing techniques: processing based on spectral vegetation indices (SVIs), texture measures, and combinations of SVIs with textural analyses. They found that SVI-based approaches did not yield reliable LAI estimates, accounting for at best 68% of the observed variation in LAI; texture-based methods were somewhat better, explaining up to 72% of the observed variation; however, a combination of the two approaches yielded an even better adjusted R^2 value of 0.84. The authors demonstrated that the accuracy of estimated LAI values based on remote-sensing data could be significantly increased by considering textural information. Based on the relatively extensive literature review above regarding spatial information derived from high resolution satellite imagery, it has been shown that textural information is unique and can be very useful in estimating and mapping plant LAI.

Developed in recent years, high resolution WorldView series sensors that can produce even higher spatial and spectral resolution satellite image data compared to IKONOS and QuickBird sensors, are expected to provide a greater potential for predicting and mapping forest structural parameters than other high resolution sensors (e.g., IKONOS and QuickBird). However, although the WV2 data have been utilized for estimating and mapping many forest structure parameters including biomass, basal area (BA), number of trees (NT), stem volume (SV), mean diameter at breast height (MDBH), mean tree height (MTH), etc., based on our literature review, there were no studies on estimating and mapping forest LAI using the WV2 data. For example, in predicting forest structural parameters such as NT, BA, SV, Gini coefficient (GC), and standard deviation of DBH (SDDBH), etc. using the image textural information derived from WV2 multispectral (MS) bands in a dryland forest, Israel, cross-validated statistics confirmed that structural parameters including BA, SDDBH, and GC could be predicted and mapped with a reasonable accuracy (Ozdemir and Karnieli, 2011). In estimating and mapping pine plantation structure parameters (volume, BA, DBH and MTH) using WV2 MS images, Shamsoddini et al. (2013) also demonstrated that estimate models derived from textural attributes of eight spectral bands provided the best estimates of the four forest structural parameters, compared to those derived from four typical bands and the models derived from spectral derivatives. Based on the demonstrated power and potential of textural information derived from WV2 data for estimating and mapping forest structural parameters and considering even higher spatial /spectral resolution of WV2 data, it is necessary to test and evaluate the power and potential of textural information extracted from the WV2 MS imagery for estimating and mapping a mixed natural forest LAI.

Therefore, the overall focus of this study is on exploring the potential of the new high spatial/spectral resolution WV2 satellite imagery for estimating and mapping forest LAI in a mixed natural forest area in Florida, USA. For this case, all possible spectral / spatial features (SFs) including spectrum-based features and texture-based features were first extracted from WV2 MS bands and Landsat TM imagery (spectrum-based SFs only), selected and tested; and then a canonical correlation analysis (CCA) with different sets of selected SFs was used to evaluate relationships between sets of SFs and LAI measurement to estimate and map forest LAI. The substantial objectives of this study include: (1) selecting and evaluating SFs extracted from WV2 MS bands and TM data for estimating and mapping forest LAI; and (2) comparing LAI mapping accuracies (a) from spatial resolutions between 2-m WV2 MS data and 30-m TM imagery, (b) from the nature of SFs between spectrum-based features and texture-based features, and (c) from sensors between TM and WV2. The expected novel significance of this study is first demonstrating the potential of the newly developed high spectral/spatial resolution WV2 sensor for improving the accuracy of estimating and mapping forest LAI using textural information derived from the WV2 MS bands compared with using spectrum-based features only. Relevant issues associated with effects of window size and spectral bands for extracting textural information on estimating forest LAI will also be discussed.

STUDY SITE AND DATA SETS

Study Site

The study area that includes the University of South Florida Ecological Research Area (USF Eco-Area) and its surrounding areas at approximately 28° N and 82° W is presented in Fig. 1. It is within the City of Tampa, Florida, USA. Over half of the study area is composed of floodplain wetlands associated with Cypress Creek and the Hillsborough River. The rest of it is composed of natural and developed uplands. Based primarily upon the Florida

Natural Areas Inventory and Department of Natural Resources classification system (FNAI and DNR 1990) and Schimdt (2005) field observations, major natural plant community types consist of riverine communities, palustrine communities, terrestrial communities, and rural/developed plant communities. For detailed descriptions of plant communities and climate and topographic conditions in the study area, see Pu (2012) and Schimdt (2005).

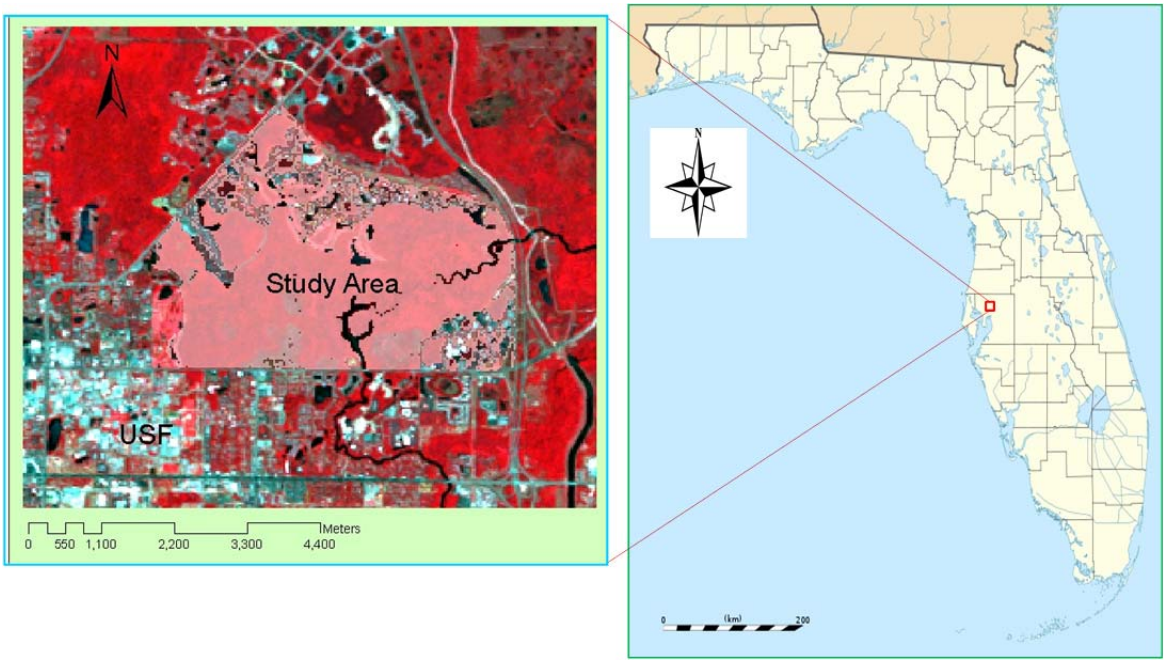

Fig. 1. Location map of the study area, presented in a false color composite image made using TM bands 4, 3, and 2 for RGB, acquired on April 30, 2011. The study area, masked in a transparent area, covers University of South Florida Ecological Research Area (USF Eco-Area) and its surrounding areas.

Data Acquisition and Measurement

WorldView-2 (WV2) imagery. The WV2 satellite imagery (DigitalGlobe, Inc., USA) was acquired on May 1, 2011 at an average off nadir view angle of 29.4°. WV2 is the first commercial eight MS band high resolution satellite (sensor) with a swath width of 16.4 km, a revisit time of 1.1 average days, and a spatial resolution of 2 m for eight MS bands: Coastal blue (Band1, 400 – 450 nm), Blue (Band2, 450 – 510 nm), Green (Band3, 510 – 580 nm), Yellow (Band4, 585 – 625 nm), Red (Band5, 630 – 690 nm), Red-edge (Band6, 705 – 745 nm), NIR1 (Band7, 770 – 895 nm) and NIR2 (Band8, 860 – 1040 nm). The satellite also has a panchromatic sensor (Pan, 450 – 800 nm) with about 0.5 m spatial resolution that was not used in this study. According to DigitalGlobe (2009), the eight bands are uniquely chosen to meet the needs of a variety of applications, including resources management, coastal mapping, environmental monitoring, infrastructure mapping, and others.

Landsat 5 TM data. One scene of Landsat TM imagery (path 17 / row 41) was acquired on April 30, 2011, covering the study area. The TM imagery in GeoTIFF Level 1 format was directly downloaded from the USGS site: http://glovis.usgs.gov/. TM bands 1-5 and 7 of the scene were used in this analysis.

LAI collection. An LAI-2000 Plant Canopy Analyzer (PCA) was used to measure LAIs in the field. A total of 70 LAI measurements were taken on April 8, 2008. At the same plot locations used for measuring LAIs on April 8, 2008, another 70 LAI measurements were re-taken on April 20, 2010. The LAI measurement taken by the PCA has been termed, 'effective' LAI (White et al., 1997). The LAI plots were separately deployed over lowland and upland subareas. The number, mean, standard deviation and range of LAI measurements taken from 2008 and 2010 in the two subareas are summarized in Table 1 in association with a list of relevant plant community types. Each LAI measurement represents an average of ten PCA readings which were taken in a plot area ranging from 1000 to 2000 m^2. After taking an LAI measurement, the plot's exact location was marked on an IKONOS color composite image that was acquired on April 6, 2006 based on surface features.

Table 1. Summary of LAI measurements, taken on Apr. 8, 2008 (Apr08)

and Apr. 20, 2010 (Apr10) used in this analysis.

Types	Apr08 LAI measurements				Apr10 LAI measurements				Relevant plant communities*
	Number	Mean	SD	Range	Number	Mean	SD	Range	
Lowland	21	3.16	0.67	2.57	21	3.12	0.64	2.55	Floodplain swamp, Floodplain marsh, partial Floodplain forest, and Black water community types
Upland	49	2.19	0.77	3.30	49	2.28	0.75	3.48	Mesic flatwoods,Floodplain forest, sandhill, Hydric hammock, Xeric hammock, Scrubby flatwoods, Wet flatwoods, seepage slope, and Ruderal/developed community types
Overall	70	2.48	0.86	3.81	70	2.53	0.81	3.62	All plant community types

* Referred to FNAI and DNR (1990) and Schmidt (2005). SD denotes standard deviation.

Based on the existing available data sets (satellite imagery and *in situ* LAI measurements) described above for this analysis, WV2 and TM imagery were acquired one year later on approximately the same date as for collecting *in situ* LAI measurements (i.e., April 20, 2010). This time difference between field LAI measurement and acquisition of both WV2 and TM imagery did not affect our analyses below because the LAI in a study area with mixed natural forests does not change significantly in one year, within the same season. Since the *in situ* LAI measurements collected on April 8, 2008 were also taken at the same plots as for LAI measurements taken on April 20, 2010, we can make a comparative analysis between the two sets of LAI measurements for the two year difference. Fig. 2 clearly illustrates that no significant LAI change can be observed from the scatterplot. Those scatter points off the 1:1 diagonal line could be caused by a field sampling error. Given the only one year difference (within the same season) between 2010 and 2011, for this study, any change of LAI measurement for the one year might be ignored.

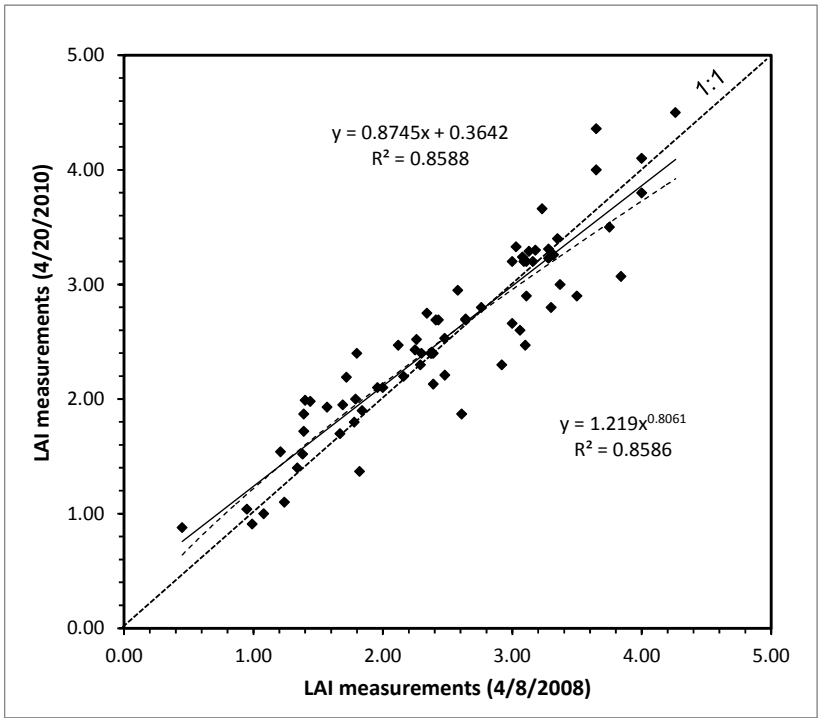

Fig. 2. Scatter plot showing linear and nonlinear relationships between LAIs measured on April 8, 2008 and April 20, 2010.

METHODOLOGY

Fig. 3 presents a flowchart of analysis methods to estimate and map forest LAI by using band reflectance, VIs and spatial information derived from WV2 and TM imagery. The WV2 and TM imagery was first atmospherically corrected. All potential spectral/spatial features (SFs) were then extracted from WV2 and TM data and tested, and a CCA algorithm was performed with inputs of selected SFs and *in situ* LAI measurements to create one canonical variable. Finally linear regression models were simulated with canonical variable 1 against *in situ* LAI measurement and used to predict and map pixel-based forest LAI.

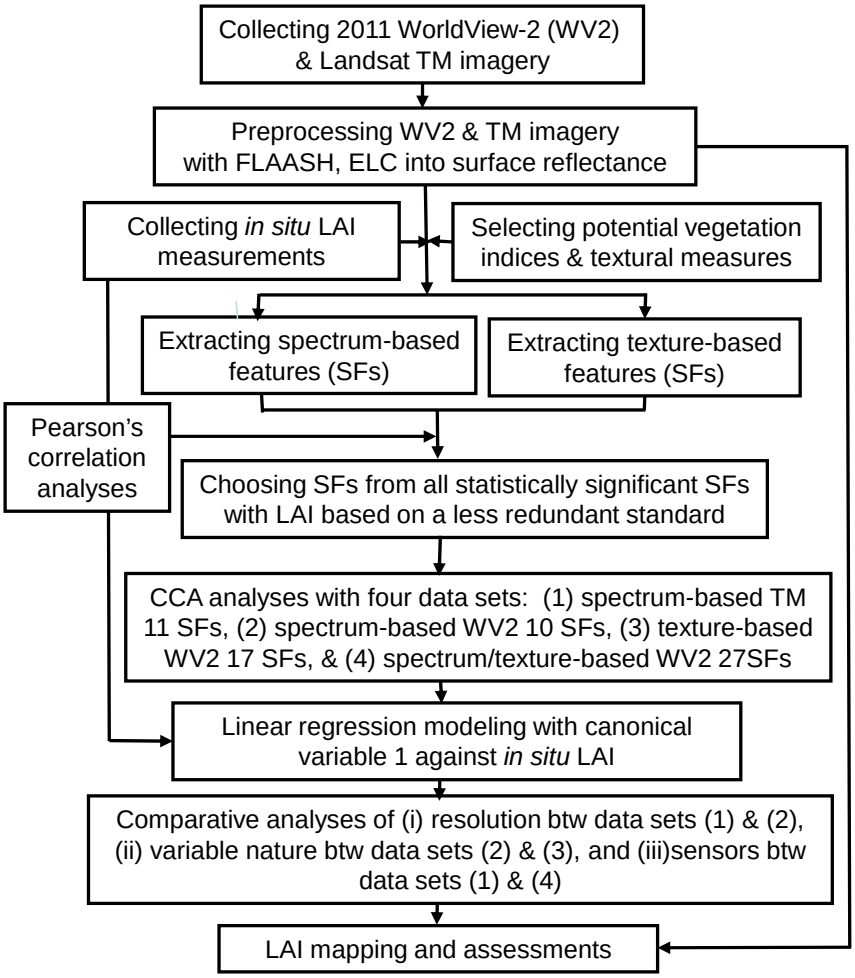

Fig. 3. Flowchart of the analysis procedure of LAI mapping and assessment with spectrum/texture-based features (SFs) extracted from Landsat TM and high resolution WV2 imagery. CCA represents canonical correlation analysis.

Image Preprocessing

Per WV2 MS image data, based on the comparative result of three atmospheric correction methods applied to the WV2 MS data in Pu et al., (2015), the atmospheric correction result created with empirical line calibration (ELC) method was used in this analysis. Per TM imagery, since the *in situ* spectral measurements from both bright and dark targets were not available, we utilized the FLASSH (Fast Line-of-sight Atmospheric Analysis of Spectral Hypercubes) method to correct atmospheric effects for the TM imagery (see Pu (2012) for the detailed FLASSH atmospheric correction procedure). As a result, all six TM bands (TM 1-5 and 7) in radiance were converted to surface reflectance in the study area. Neither WV2 image nor TM image was geometrically corrected because the study area is relatively level and small (approximately 13 km^2) but registration was conducted between them.

Spectral/Spatial Feature Extraction and Selection

To use reflectance and textural information derived from both WV2 and TM imagery for estimating and mapping forest LAI, two types of features (variables) (SFs): spectrum-based features and texture-based features were extracted from WV2 imagery but only one type spectrum-based features from TM data. The spectrum-based features include band reflectance and various VIs (Table 2, 12 VIs and six band reflectances from TM data while 13 VIs and eight band reflectances from WV2 imagery). In this study, per TM data, the 12 VIs consist of nine 2-band VIs and three 3-band VIs (Table 2). The reason we chose the 12 VIs extracted from TM data (also among them, nine VIs from WV2 data) is that they have been effectively and successfully used to estimate and map forest canopy LAI from moderate and high resolution multispectral remote sensing data (e.g., Colombo et al., 2003; Soudani et al., 2006; Song and Dickinson, 2008; Kraus et al., 2009; Gray and Song, 2012; Gu et al., 2012; Zhou et al., 2014). For the WV2 data, the 13 VIs consist of nine VIs that are the same as those constructed from TM data and four NDVI-like VIs (Table 2). Accordingly, we can base the same reasons as aforementioned to use the nine VIs in this analysis. The other four NDVIs were selected according to the studies by Cavayas et al. (2012) and Pu and Landry (2012).

A total of 13 texture-based features were selected and extracted from the eight WV2 MS bands in this analysis, comprising five 1^{st}-order grey level statistical texture measures and eight 2^{nd}-order grey level statistical texture measures (Table 3). The selection of the 13 texture-based features was based on literature review and their potential for estimating and mapping forest structural parameters including LAI from high resolution MS data, which has been demonstrated in many existing studies (e.g., Kraus et al., 2009; Murray et al., 2010; Gebreslasie et al., 2011; Ozdemir and Karnieli, 2011; Gómez et al., 2011, 2012; Gu et al., 2012, 2013; Shamsoddini et al., 2013; Zhou et al., 2014). The 1st-order statistical texture measures are derived from the pixel values in a moving window with different window sizes, but don't consider the spatial relationships among pixels within a window. The 2nd-order statistical texture measures are calculated from the spatial-dependency gray-level co-occurrence matrices (GLCM) describing the probability of each pair of pixel values co-occurring in a given direction and distance (Haralick et al., 1973). In this study, to assess the effects of the window size (for both 1^{st}- and 2^{nd}-order texture measures) and direction (for 2^{nd}-order texture measures only) on the power of texture-based features to estimate forest LAI, based on literature review, four window sizes (3×3, 5×5, 7×7, and 9×9) and four directions (0^o, 45^o, 90^o, and 135^o) were tested with WV2 Band5 (typical Red band). The reasons for choosing Band5 to test the effects were (1) the workload was too heavy to test all window sizes and directions for all eight WV2 bands, and (2) per preliminary correlation analyses of band reflectances with LAI measurements (Table 2), Band5 produced the best correlation with LAI. In this testing, we first determined the window size with a fixed direction 0^o based on correlations of texture-based features with measured LAI, and then determined a direction with a selected window size for GLCM calculation. After the best window size and direction with Band5 were determined, the window size and direction were then applied to all other WV2 MS bands.

To reduce redundancy and data dimensionality without losing significant useful spectral and spatial information, it is necessary to select a subset of SFs from the total of 18 spectrum-based features extracted from TM data and the total of 125 SFs (21 spectrum-based features and 104 texture-based features) from WV2 data prior to canonical correlation analysis (CCA) to produce low dimensionality CCA transformed variables (see below). To do so, we first calculated Pearson's correlation R^2 value for each SF with LAI measurement and retained all SFs with R^2 value > $R^2_{(0.001,df=68)} = 0.1482$, we then calculated Pearson's correlation R^2 value between any two SFs separately from three groups of retained SFs: (1) retained spectrum-based features from TM data, (2) retained spectrum-based features and (3) retained texture-based features from WV2 data. Per any pair of retained SFs, if there exists a high correlation of $R^2 \geq 0.9$ from groups 1 and 2, and $R^2 \geq 0.8$ from group 3, then one SF with a relatively higher R^2 with LAI measurement would be retained (Zhang et al., 2014). By examining all possible combinations of any two SFs with this procedure, the retained SFs selected for further CCA processing would ensure a relatively low redundancy level.

Canonical Correlation Analysis (CCA)

CCA is one technique of multivariate analyses, which evaluates the relationship between two sets (or groups) of variables. Each set can contain multiple variables. Given the two sets of variables (e.g., a set of SFs extracted from remote sensing images and the other set of forest biophysical variables, LAI, biomass, etc.), CCA finds corresponding pairs of linear combinations from the original two groups of variables, called canonical variables. The first pair of linear combinations is the one with the largest correlation and the two linear combinations are called the first pair of canonical variables (SAS, 1991; Nielsen, 2002). The second pair of linear combinations is the one with the second largest correlation, subject to the condition that they are orthogonal to the first pair of canonical variables, and the two linear combinations are called the second pair of canonical variables. Higher order canonical correlations and canonical variables are defined similarly (Nielsen, 2002). When there is only one variable in a set

Table 2. Summary of 16 vegetation indices, 8 bands of WV2, and 6 bands of TM tested in this analysis.

Index	Formula	References	WV2		TM	
			Bands	R^2	Bands	R^2
SR	ρ_{NIR} / ρ_R	Baret and Guyot, 1991; Jordan 1969.	Band5, Band7	0.4894	TM3, TM4	0.5047
NDVI	$(\rho_{NIR} - \rho_R)/(\rho_{NIR} + \rho_R)$	Fassnacht et al., 1997; Rouse et al., 1973	Band5, Band7	0.5268	TM3, TM4	0.4663
PVI	$\frac{1}{\sqrt{a^2+1}}(\rho_{NIR} - a\rho_R - b)$ a = slope of the soil line b = soil line intercept	Baret and Guyot, 1991; Huete et al., 1985.	Band5, Band7	0.4245	TM3, TM4	0.5060
SAVI	$\frac{(\rho_{NIR} - \rho_R)(1+L)}{(\rho_{NIR} + \rho_R + L)}$ L = a correction factor	van Leeuwen and Huete, 1996; Huete 1988.	Band5, Band7	0.4878	TM3, TM4	0.5624
NLI	$(\rho_{NIR}^2 - \rho_R)/(\rho_{NIR}^2 + \rho_R)$	Gong et al., 2003; Goel and Qin, 1994.	Band5, Band7	0.5269	TM3, TM4	0.5191
MSR	$\frac{(\rho_{NIR}/\rho_R - 1)}{(\rho_{NIR}/\rho_R)^{1/2} + 1}$	Gong et al., 2003; Chen, 1996.	Band5, Band7	0.5173	TM3, TM4	0.5067
TSAVI	$\frac{a(\rho_{NIR} - a\rho_R - b)}{[a\rho_{NIR} + \rho_R - ab + X(1+a^2)]}$	Gong et al., 2003; Baret and Guyot, 1991	Band5, Band7	0.4329	TM3, TM4	0.5101
NDMI	$(\rho_{NIR} - \rho_{SWIR})/(\rho_{NIR} + \rho_{SWIR})$	Hardisky et al., 1983	n/a	n/a	TM4, TM5	0.4181
ARVI	$(\rho_{NIR} - \rho_{rb})/(\rho_{NIR} + \rho_{rb})$ $\rho_{rb} = \rho_R - \gamma(\rho_B - \rho_R)$	Kaufman and Tanré, 1992	Band2, Band5, Band7	0.5384	TM1, TM3, TM4	0.4646
EVI	$G\frac{(\rho_{NIR} - \rho_R)}{(\rho_{NIR} + C_1\rho_R - C_2\rho_B + L)}$	Huete et al., 1999	Band2, Band5, Band7	0.4786	TM1, TM3, TM4	0.5646
RSR	$\frac{\rho_{NIR}}{\rho_R} \bullet \frac{(\rho_{SWIR\text{-}max} - \rho_{SWIR})}{(\rho_{SWIR\text{-}max} - \rho_{SWIR\text{-}min})}$	Brown et al., 2000	n/a	n/a	TM3, TM4, TM5	0.4790
ISR	ρ_{NIR} / ρ_{SWIR}	Fernandes et al., 2002	n/a	n/a	TM4, TM5	0.4205
NDVI2	$(\rho_{NIR} - \rho_{Red-edge})/(\rho_{NIR} + \rho_{Red-edge})$	Pu and Landary, 2012	Band6, Band8	0.4008	n/a	n/a
NDVI3	$(\rho_{NIR} - \rho_Y)/(\rho_{NIR} + \rho_Y)$	Pu and Landary, 2012	Band4, Band8	0.4970	n/a	n/a
NDVI4	$(\rho_{Red-edge} - \rho_C)/(\rho_{Red-edge} + \rho_C)$	Pu and Landary, 2012	Band1, Band6	0.1674	n/a	n/a
NDVI5	$(\rho_{Red-edge} - \rho_R)/(\rho_{Red-edge} + \rho_R)$	Pu and Landary, 2012	Band5, Band6	0.4380	n/a	n/a
Note:			Band1	0.1777	TM1	0.1874
(1). $\rho_B, \rho_R, \rho_{NIR}$ and ρ_{SWIR} are denoted as reflectances in blue (TM1, Band2),			Band2	0.2749	TM2	0.2881
red (TM3, Band5), near-infrared (TM4, Bands 7&8) and short wave			Band3	0.3211	TM3	0.3624
infrared (TM5) wavelengths, while ρ_C, ρ_Y, and $\rho_{Red-edge}$			Band4	0.4088	TM4	0.4541
represent reflectance in coastal (Band1), yellow (Band4) and red-edge (Band6).			Band5	0.4881	TM5	0.2102
(2). All R^2 values were calculated with in situ LAI measurements and			Band6	0.0215	TM7	0.2296
corresponding VIs are statistically significant at 0.999 confidence level			Band7	0.3673		
($R^2_{(0.001,df=68)}$ = 0.1482) except WV2 Band6.			Band8	0.3162		

Table 3. A list of 1st- and 2nd-order texture measures*, extracted from eight WV2 MS bands and used in this analysis.

Name	Texture measure	Formula
1st-order texture measures (five):		
B#RAN1	Data Range	$\max\{X\}-\min\{X\}$
B#MEA1	Mean	$\sum_{i=0}^{N-1} ip_i = S_M$
B#VAR1	Variance	$\sum_{i=0}^{N-1} (i-S_M)^2 p_i = S_D^2$
B#ENT1	Entropy	$\sum_{i=0}^{N-1} p_i(-\ln p_i)$
B#SKE1	Skewness	$\frac{1}{S_D^3}\left[\sum_{i=0}^{N-1}(i-S_M)^3 p_i\right]$
2nd-order texture measures (eight):		
B#MEA2	Mean	$\sum_{i=0}^{N-1} ip(i,j) = \mu$
B#VAR2	Variance	$\sum_{i,j=0}^{N-1} p(i,j)(i-\mu)^2$
B#HOM2	Homogeneity	$\sum_{i,j=0}^{N-1} \frac{p(i,j)}{1+(i-j)^2}$
B#CON2	Contrast	$\sum_{i,j=0}^{N-1} p(i,j)(i-j)^2$
B#DIS2	Dissimilarity	$\sum_{i,j=0}^{N-1} p(i,j)\lvert i-j\rvert$
B#ENT2	Entropy	$\sum_{i,j=0}^{N-1} p(i,j)(-\ln p(i,j))$
B#ASM2	Angular Second Moment	$\sum_{i,j=0}^{N-1} p(i,j)^2$
B#COR2	Correlation	$\sum_{i,j=0}^{N-1} p(i,j)\frac{(i-\mu_i)(j-\mu_j)}{\sqrt{\sigma_i^2\sigma_j^2}}$

Note: B# represents band number of WV2 MS imagery. Per the 1st-order textures, p_i is relative frequency of grey level i in the pixel window; X is pixel value (grey level) in the window; N is the number of gray levels. Per the 2nd-order textures, i, j are the row/column numbers in a spatial-dependency matrix; p(i,j) is the value in the cell i,j in the matrix; N is the number of rows or columns and equals to the number of grey levels.

*: Haralick et al., 1973; Anys and He, 1995; Lu and Batistella, 2005; Kraus et al., 2009; Zhou et al., 2014.

of original variables (e.g., a biophysical variable, LAI in this study) and the other set of variables are multiple variables (e.g., a set of SFs), CCA only provides a set of transformation coefficients for the multiple variables (SFs) that align the coefficients with the variation of the variable (LAI). In this study, the SAS CANCORR procedure (SAS, 1991) was applied to implement CCA to estimate and map forest LAI from the SFs extracted from TM and WV2 images. During the implementation of the CCA procedure in SAS, the input data (i.e., SFs and LAI) first needed to be standardized.

Estimating and Mapping Forest LAI

In this analysis, based on the dimensions and properties of input variables, one canonical variable for one set of SFs using CCA procedure (SAS, 1991) with 70 samples was produced. The canonical variable was then used to develop a corresponding linear regression model with LAI measurement to estimate and map pixel-based forest LAI. For estimating and mapping the pixel-based LAI from each set of SFs, the corresponding pixel based canonical variable was first calculated with a corresponding set of SF values in standardized format. The developed four linear regression models then were used for calculating pixel-based LAI values from the corresponding sensors' data.

Accuracy Assessment Criteria

The coefficient of correlation (R^2), root mean square error (RMSE), and cross-validation (CV) RMSE (SAS, 1991) were used as accuracy assessment criteria to assess the degree of correlation between two variables, estimation accuracy, and prediction capability for estimating and mapping forest LAI associated with different spectral variables and textural feature extraction methods. The R^2 can be calculated from a Pearson's correlation

definition. The RMSE can be defined as $RMSE = \sqrt{\frac{\sum_{i=1}^{n} (y_i - \hat{y}_i)^2}{n}}$, where, $y_i (i = 1,2,\ldots,n)$ are actual LAI measurements; $\hat{y}_i (i = 1,2,\ldots,n)$ are LAI values estimated from a linear regression model; n is the number of samples. The CV RMSE is calculated via iteratively generating regression models with *n-1* samples while reserving one sample from the input data set (rotating *n* times) for testing a corresponding regression model.

RESULTS

Correlation Analyses of Individual SFs with LAI

Per TM data, a Pearson's correlation (R^2) was calculated between ground measured LAI and each of the 18 spectrum-based features (6 single TM band reflectances and 12 VIs) using 70 samples (Table 2). All R^2 values are statistically significant at $\alpha = 0.001$. For all 12 VIs, all R^2 values are higher than those for all six single TM bands except for NDMI (Normalized Difference Moisture Index) and ISR (Infrared Simple Ratio index) that with TM5 (SWIR) did not produce a higher R^2 compared to that with single band TM4 (NIR) only. Compared with the correlation results created with spectrum-based features from TM data, most WV2 single bands and VIs have produced similar correlation results except three additional NDVI# (NDVI2, NDVI4 and NDVI5). Per the correlation results created with all WV2 MS bands, we have noted that Band5 (Red) has produced the highest R^2 value, even higher than that with TM4 (NIR). Consequently, the WV2 Band5 has been used to test to determine the best window size and direction for extracting texture-based features from all WV2 MS bands.

Testing was conducted to determine an appropriate window size for extracting five 1st-order statistical texture measures (Table 3) from every WV2 MS band. Fig. 4(a) presents the testing results with WV2 Band5 and four window sizes: 3×3, 5×5, 7×7, and 9×9. Per Fig. 4(a), in considering all five texture measures, the 3×3 window size has generated the best result. With a fixed direction of 0^o, Fig. 4(b) illustrates the testing results of eight 2nd-order statistical texture measures (Table 3) with WV2 Band5 and four window sizes: 3×3, 5×5, 7×7, and 9×9. As can be seen in the figure, the 9×9 window size created a relatively better R^2 across the eight texture measures. Therefore, with the fixed 9×9 window size, we further tested the effects of four directions (0^o, 45^o, 90^o, and 135^o) on R^2 value with the eight texture measures extracted from WV2 Band5. The testing results of the eight texture measures with each of the four directions are shown in Fig. 4(c). As seen in Fig. 4(c), the direction 90^o has led to a better R^2 value compared to the other directions. Based on the testing results aforementioned, the 3×3 window size might be used to calculate the five 1st-order texture measures, and the 9×9 window size with a direction of 90^0 might be used to calculate the eight 2nd-order texture measures from all eight WV2 bands. Fig. 5 presents correlation analysis results of all 13 texture-based features extracted from all eight WV2 bands with ground measured LAI. By comparing the correlation analysis results of the 13 texture measures among the eight WV2 bands, for both 1st-order and 2nd-order texture measures, it was observed that the eight WV2 bands could be divided into two groups based on their corresponding R^2 values: a visible band group (Bands 1-5) and a Red-edge and NIR group (Bands 6-8). The 13 texture-based features extracted from the visible band group have produced higher R^2 values compared with those created from the Red-edge and NIR band group.

CCA Processing

To conduct CCA processing, there are four data sets of predictor SFs as input data with only one response variable, LAI: (Set1) 11 spectrum-based features from TM data; (Set2) 10 spectrum-based features from WV2 data; (Set3) 17 texture-based features from WV2 data; and (Set4) 27 pooled spectrum-/texture-based features from WV2. Table 4 shows substantial retained SFs for the four data sets after reducing redundancy among the potential SFs (see section 3.2 above). Consequently, based on the principle of the CCA algorithm and the four sets of SFs with one biophysical variable LAI, only one set of transformation coefficients for one set of SFs can be produced in this study. By using the transformation coefficients, one canonical variable for each set of SFs can be calculated, which will be correlated to LAI measurement to model and map pixel-based LAI.

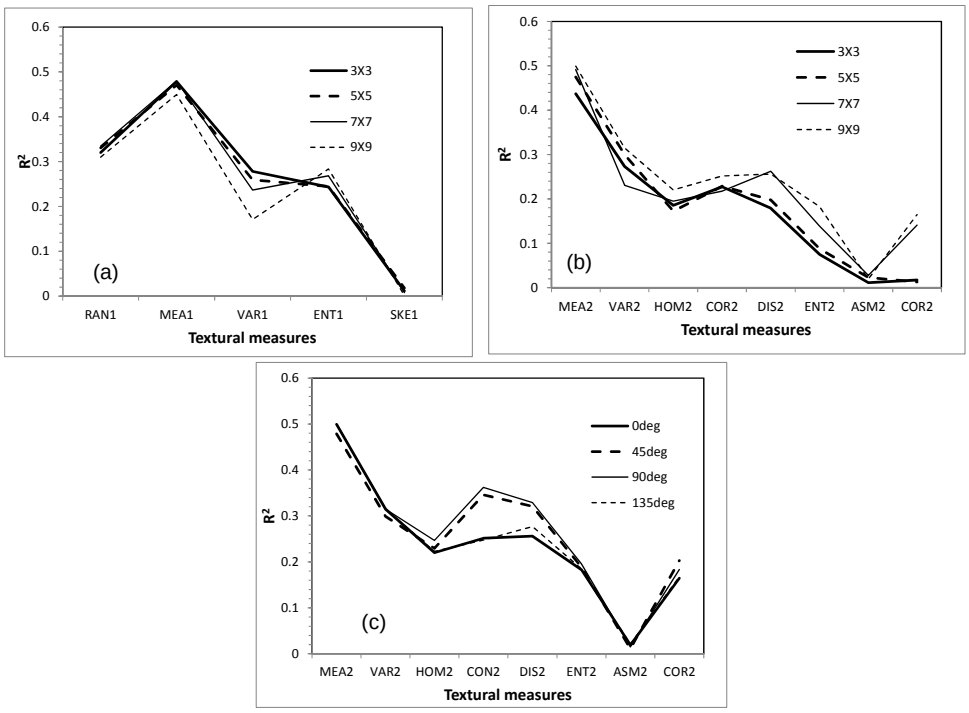

Fig. 4. Comparisons of coefficients of correlation (R2) of texture measures with LAI measurement among four window sizes (3×3, 5×5, 7×7 and 9×9) and among four directions (0°, 45°, 90° and 135°). (a) WV2 band 5 with five 1st order texture measures and four window sizes; (b) WV2 band 5 with eight 2nd order texture measures, four window sizes and direction 00; (c) WV2 band 5 with eight 2nd order texture measures, four directions and window size 9×9.

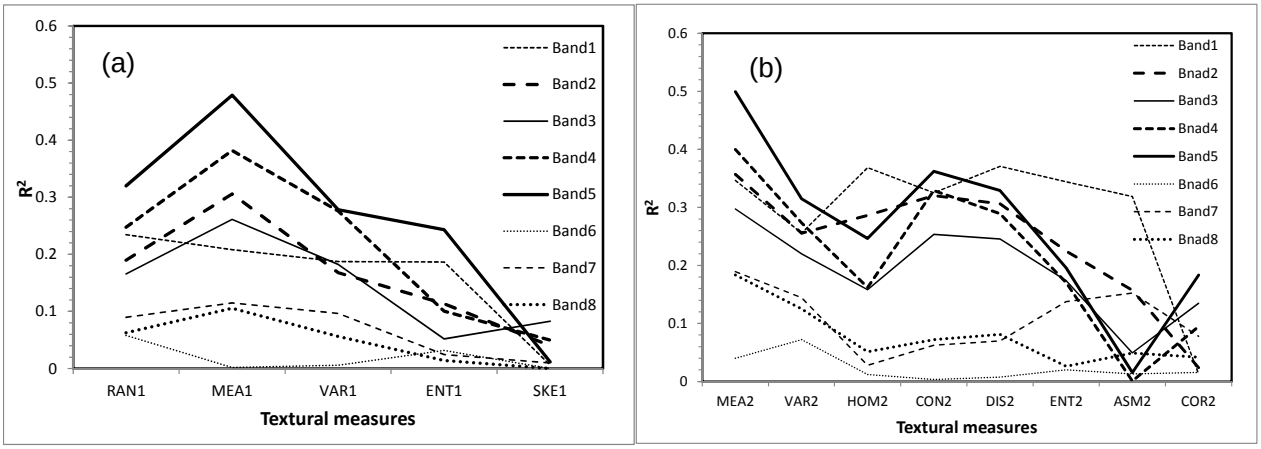

Fig. 5. Comparisons of coefficients of correlation (R2) of texture measures with LAI measurement among the eight WV2 MS bands. (a) R2 values were created with five 1st order texture measures with window size 3×3 and (b) with eight 2nd order texture measures with window size 9×9 and direction 90°.

Table 4. A summary of spectral features (SFs) selected for conducting CCA analysis.

Data sets	SFs
(Set1) TM 11 spectrum-based SFs	TMs 1, 2, 3, 5, 7, SR, SAVI, NLI, TSAVI, EVI, ISR
(Set2) WV2 10 spectrum-based SFs	Bands 1, 2, 3, 4, SAVI, NLI, MSR, ARVI, NDVI2, NDVI3
(Set3) WV2 17 texture-based SFs	B1RAN1, B1ENT1, B5RAN1, B5MEA1, B5ENT1, B1DIS2, B2CON2, B2DIS2, B3DIS2, B3ENT2, B4DIS2, B4ENT2, B5MEA2, B5VAR2, B5CON2, B5COR2, B8MEA2
(Set4) WV2 27 spectrum/texture-based SFs	SFs from Set2 and Set3

Fig. 6 presents four scatter plots created with standardized canonical variable 1 against standardized LAI measurements. All plots in Fig. 6 show significant linear relationships between canonical variable 1 and LAI. Per the four plots, it is clearly illustrated that (1) canonical variable 1 derived from Set2 has produced better correlation with LAI compared to that derived from Set1 (R^2 = 0.64 vs. 0.59); (2) canonical variable 1 derived from Set3 has produced higher correlation with LAI compared to that derived from Set2 (R^2 = 0.69 vs. 0.64); and (3) canonical variable 1 derived from Set4 has resulted in much higher correlation (R^2 = 0.84) with LAI compared to either the one derived from Set2 or Set3. These results demonstrate that the textural information extracted from the high resolution WV2 data can be used to account for more spatial variation of the LAI measurements in the 70 samples to improve the accuracy of estimating forest LAI. In addition to using the R^2 values to evaluate the linear correlations with the four sets of SFs, RMSE and CV-RMSE indices (Table 5) were also used to evaluate the quality of the four linear regression models. From this evaluation it can be concluded that the linear regression model created with Set4 of SFs is best.

LAI Mapping with Canonical Variable 1

To estimate and map pixel-based forest LAI, the pixel based canonical variable values were first calculated with corresponding four sets of linear transformation coefficients calculated by CCA from the four sets of SFs in standardized format (ENVI4.8, 2012). Then the four linear regression models between the canonical variable and LAI, shown in Figure 6, were used to calculate pixel-based LAI values. Fig. 7(a) presents an LAI map produced by using Set1 of SFs and Fig. 7(b) and Fig. 7(c) present LAI maps created by respectively using Sets 2 and 3 of SFs while Fig. 7(d) shows an LAI map produced by using Set4 of SFs. The LAI maps were made with TM4 image in grayscale as their background. In general, all LAI maps clearly show the spatial variation of LAI with low LAI values distributed in patches close to the southern boundary, located west and east of Hillsborough River in orange/red color. These areas with relatively low LAI were mostly distributed by several terrestrial communities, including sandhill, xeric hammock, and mesic flatwoods communities. The residential areas, located towards the southeast corner and close to the north boundary of the study area, also had a low LAI value in red to orange. Street trees are distributed throughout this residential area. The areas with higher LAI value within the study area, in the light yellow to green color, were occupied by several palustrine communities, including floodplain swamp, floodplain forest, floodplain marsh, and especially floodplain swamp and floodplain forest areas with LAI values mostly greater than 3.0.

Comparisons

Table 5 lists mean and standard deviation (S.D.) values of the four LAI maps, separated into two mapped areas: lowland and upland, created with Set1 of SFs from TM data, and Sets2-4 of SFs from WV2 imagery. As can be seen in the table, Sets1-3 of SFs have produced similar results (mean and S.D.) with a relatively better LAI map created with Set3 of SFs, then the one created with Set2 of SFs and a relatively less reliable one created with TM data ((Set1 data). Clearly, the pooled spectrum-/texture-based features (Set 4 of SFs) have created the best LAI map and shows greater S.D. values for the two mapped areas compared to those with Sets1-3 of SFs. Thus the results of three comparative analyses demonstrate that (1) for evaluating the effect of spatial resolution on mapping accuracy of forest LAI, the LAI map created with Set2 of SFs is more accurate than that created with Set1 of SFs; (2) for evaluating the effect of feature property on mapping accuracy of forest LAI with WV2 data, the LAI map created with Set3 is more accurate than that created with Set2; and (3) for evaluating the effect of sensors on mapping accuracy of forest LAI, obviously, the LAI map created with WV2 data (Set4) is much more accurate than that created with TM data (Set1).

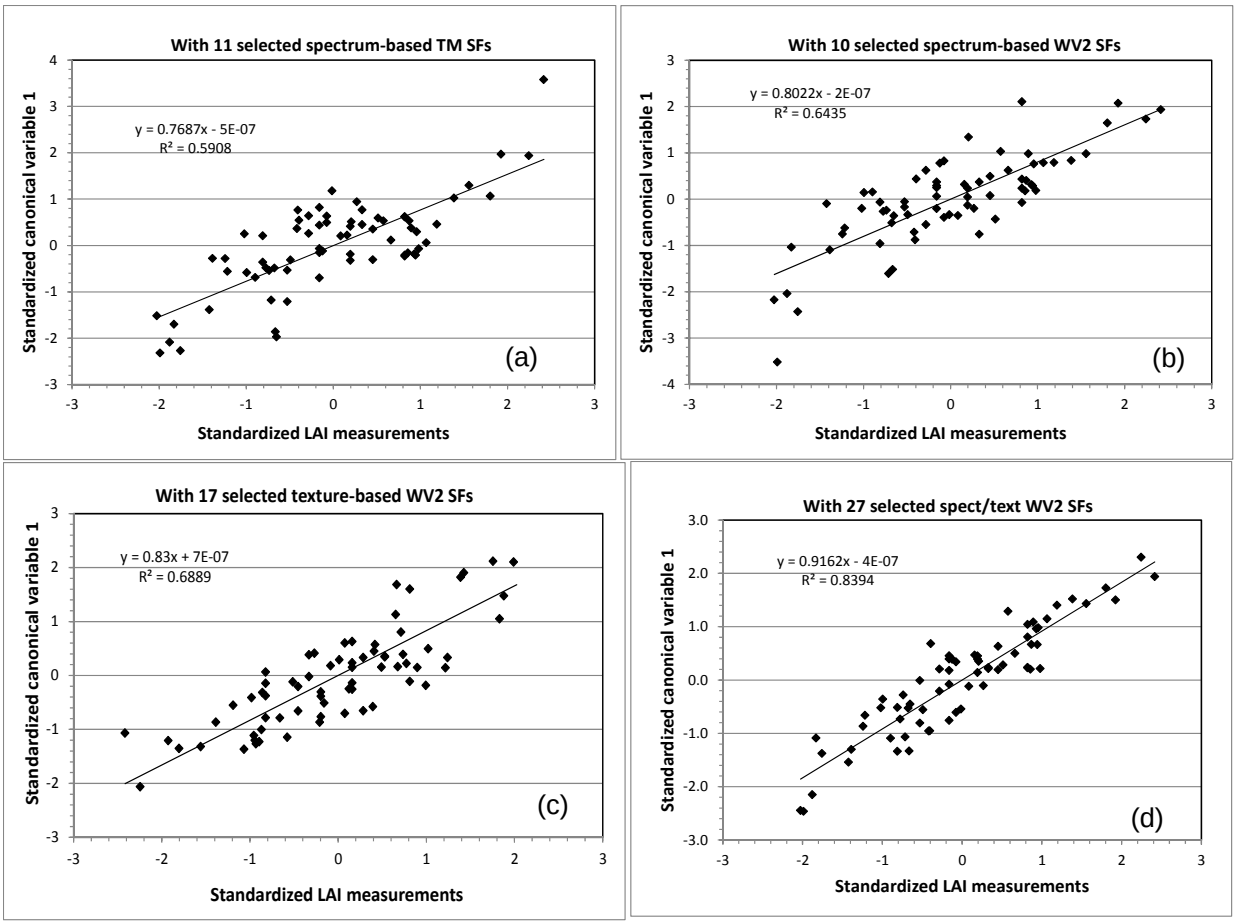

Fig. 6. Scattering plots of standardized LAI measurements (n = 70) against corresponding standardized canonical variable 1 for (a) TM data with 11 spectrum-based SFs, (b) WV2 data with 10 spectrum-based SFs, (c) WV2 data with 17 texture-based SFs, and (d) WV2 data with 27 spectrum- and texture-based SFs.

DISCUSSION

Both spectral and textural features extracted from WV2 Band6 (Red-edge) have produced very low correlation (R^2) with *in situ* LAI measurement (see Fig. 5, Table 2) in this analysis. Although we did not find any similar conclusions related to the results of WV2 Red-edge band use in existing literature, such correlation results seem reasonable because in spite of a large variation of LAI measurements (LAI: 0.88 – 4.50), a relatively small variation of Red-edge band reflectance was observed in this study. This phenomenon is understandable because the red-edge wavelength is located in the middle of Red-NIR "transition slope". Although a large variation of LAI could cause great variations of Red band and NIR band reflectances, the middle wavelength reflectance between Red and NIR is relatively "constant". Unlike a red-edge optical parameter: red-edge position, its shift (left or right shifting) is significantly related to changes of chlorophyll content (Munden et al., 1994; Belanger et al., 1995), LAI (Danson and Plummer, 1995; Pu et al., 2003), and biomass (Filella and Peñuelas, 1994), etc. Accordingly, given the relatively "constant" reflectance of the Red-edge band under varying LAI measurements, very low R^2 values for all texture-based features were also predictable.

Table 5. Summary of LAI mapping and accuracies of LAI modeling with the CCA technique.

	Mean	SD	RMSE[1]	CV-RMSE[2]
(A) LAI map with TM data (11 SFs)				
Lowland	3.03	0.670	0.6733	0.6560
Upland	2.29	1.138		
Overall	2.58	1.043		
(B) LAI map with WV2 data (10 SFs)				
Lowland	3.03	1.025	0.6034	0.6170
Upland	2.19	1.541		
Overall	2.47	1.445		
(C) LAI map with WV2 data (17 SFs)				
Lowland	3.43	0.811	0.5437	0.5774
Upland	2.17	1.544		
Overall	2.60	1.469		
(D) LAI map with WV2 data (27 SFs)				
Lowland	3.86	1.124	0.3552	0.4126
Upland	2.90	1.761		
Overall	3.22	1.641		

Note: All numbers in the table represent LAI values; S.D. is standard deviation; 1--root mean square error calculated from all 70 samples with linear regression models in Figure 5; 2--corss-validation RMSE averaged from all the 70 samples.

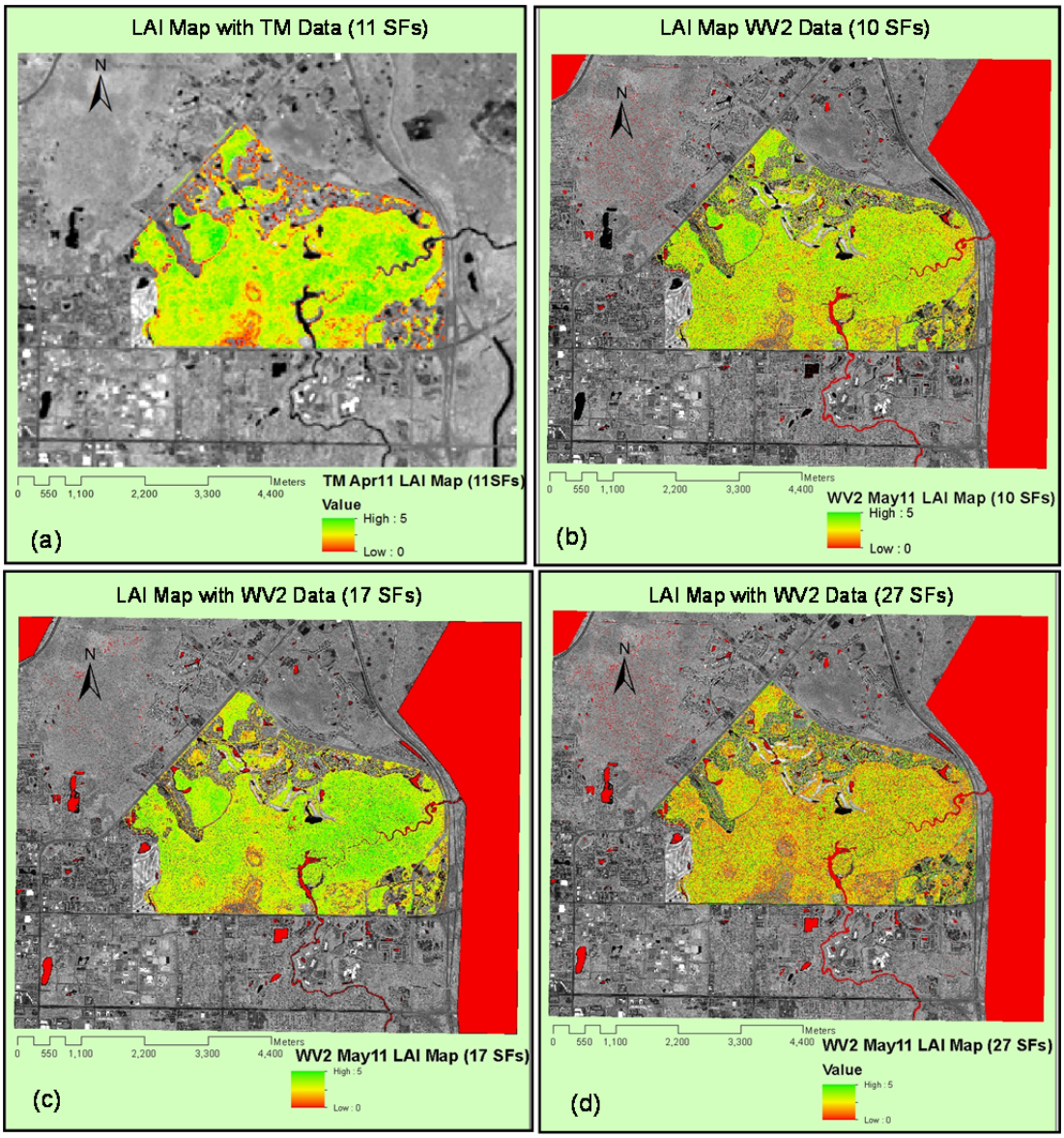

Fig. 7. A comparison of LAI maps: (a) LAI map was produced with the 11 spectrum-based SFs from the TM image and a regression model in Figure 6(a); (b) LAI map was produced with the 10 spectrum-based SFs from the WV2 image and a regression model in Figure 6(b); (c) LAI map was produced with the 17 texture-based SFs from the WV2 image and a linear model in Figure 6(c); and (d) LAI map was produced with the 27 spectrum- and texture-based SFs from the WV2 image and a linear model in Figure 6(d).

In this study, Fig. 5 (a, b) clearly illustrates that all eight WV2 MS bands could be separated into two groups: Visible band group (Bands 1-5) and NIR and Red-edge band group (Bands 6-7) based on correlation R^2 values of the individual 1^{st}- /2^{nd}-order texture measures with LAI measurement. Higher correlation R^2 values created with the visible band group than those created with the NIR and Red-edge band group were observed. Such experimental results suggest that relatively stable spectral information (with lower amplitude) derived from the visible region compared with that derived from NIR and Red-edge bands could result in the extraction of better quality texture measures from visible bands than from NIR and Red-edge bands. Existing studies on the comparison of the ability of spectral features extracted from visible bands with that from NIR bands for estimating or correlating some forest structural parameters also demonstrate what we found here, although the structural parameters do not include forest LAI. For example, Gómez et al. (2011) used spectral/spatial features extracted from QuickBird-2 imagery to estimate forest structural diversity and they found that the visible reflectance was more powerful than NIR data. In identifying forest tree species with hyperspectral measurements, Gong et al. (1997) demonstrated that the discriminating power of the visible region is stronger than the NIR region.

In this study we demonstrate that texture-based features have a higher capability to estimate and map forest LAI compared with spectrum-based features using WV2 multispectral imagery. Our experimental result confirmed some findings from previous studies. For examples, Shamsoddini et al. (2013) compared the power using 11 GLCM texture measures extracted from eight WV2 MS bands and one panchromatic (Pan) band to map forest structural parameters with spectrum-based variables. Their study showed that texture measures performed better than spectrum-based variables for estimating the forest structural parameters. Gu et al. (2012) also compared the ability of four texture measures extracted from IKONOS-2 Pan band in retrieving urban forest LAI with that of four VIs and concluded that texture measures exceeded the VIs in estimating LAI of forests with a low canopy density and regular spatial structure, in which the soil background has a strong effect on remote sensing of canopy LAI. In our study area, most of the area is covered with relatively low LAI canopy and the effect of soil background on the canopy spectrum is significant. Consequently, it should be reasonable that the texture-based features extracted from the eight WV2 bands outperformed the spectrum-based features for estimating and mapping the mixed natural forest LAI. Our and other studies' results all suggest that the detailed textural information derived from high resolution images could potentially improve estimating and mapping finer forest structural parameters.

The results of estimating and mapping forest LAI with two sensors' data demonstrate that the WV2 sensor has a greater potential for estimating and mapping forest LAI than the TM sensor. Such a general conclusion can easily be understood by the following two points. (1) Spectral and textural information extracted from the WV2 imagery should be more powerful than using spectral information extracted from TM data only in estimating and mapping forest LAI. This is because local spatial structural information of pixel values is a function of the forest structure present and the image spatial (high) resolution, and this interior relationship between forest structure and image spatial resolution provides opportunities to glean supplementary information about forests from the imagery (Falkowski et al., 2009). Therefore, such textural information extracted from the high spatial resolution image along with spectral information (e.g., band reflectance and VIs) from the image should benefit characterization of forest structural parameters, including LAI compared to using spectral information only. For example, with spectral and textural features extracted from IKONOS, Colombo et al. (2003), Song and Dickinson (2008) and Zhou et al. (2014) all demonstrated that combining both spectral and spatial information provides some improvement in estimating LAI of forest and other vegetation canopies compared with spectral information only. For estimating other vegetation structural parameters such as vegetation communities and vegetation fractional coverage, Murray et al. (2010) and Gu et al. (2013) also proved that the combination of spectral and textural information could lead to increasing estimation accuracy for these vegetation structural parameters. (2) Even using only spectral information available from both sensors, relatively high spatial resolution data from the WV2 sensor would help characterize the forest structure compared to the relatively low spatial resolution data from the TM sensor. In our study area, the experimental result of estimating LAI under a sparse stand condition with more soil background effect on canopy spectrum demonstrates this point.

CONCLUSIONS

The experimental results demonstrate that to estimate and map forest LAI, (1) using high resolution data is more accurate than using relatively low resolution data; (2) extracted from the same WV2 data, all selected texture-based features together have higher capability than that with all selected spectrum-based features together; (3) a combination of spectrum-based features with texture-based features could lead to even higher accuracy of mapping forest LAI than their either one alone; and (4) the WV2 sensor outperforms the TM sensor significantly in mapping forest LAI. In this study, since most of the area, especially in upland areas, has a sparse stand condition with LAI mostly lower than 3.0 and more soil background effect on canopy spectrum, using high resolution WV2 data might benefit mapping forest LAI. The high resolution WV2 data can offer detailed textural information that is potentially helpful to estimate and map finer forest structural parameters including LAI. Our finding of first making use of spectral and textural information extracted from WV2 data for improving forest LAI mapping will enrich current literature. Given the advantages of high resolution WV2 data (i.e., high spectral and spatial resolution features availabilities) for estimating and mapping forest LAI, it is easy to understand why the WV2 sensor outperforms TM sensor. In addition, the experimental results also indicate that the Red-edge band in WV2 has a worse performance in estimating LAI than the other WV2 bands, and WV2 MS bands in the visible range have a much better correlation with ground measured LAI than that with Red-edge and NIR bands. Since only a few studies from the existing literature could confirm our findings, and especially no studies to be found that evaluate the Red-edge band's performance for estimating forest LAI, more testing and validation work is needed, especially for different forest ecosystems.

ACKNOWLEDGEMENTS

The WorldView-2 data were provided by Dr. Shawn Landry, University of South Florida. Collection of field LAI was partially supported by University of South Florida (USF) start grant to the first author. Thanks to Ms. Barbara Nordheim-shelt, USF, for her valuable comments on the paper in its early version.

REFERENCES

Anys, H., He, D.-C., 1995. Evaluation of textural and multipolarization radar features for crop classification. Transactions on Geoscience and Remote Sensing 33(5),1170-1181.

Baret, F., Guyot, G., 1991. Potentials and Limits of Vegetation Indices for LAI and APAR Assessment. Remote Sensing of Environment 35, 161-173.

Belanger, M. J., Miller, J. R., Boyer, M. G., 1995. Comparative relationships between some red edge parameters and seasonal leaf chlorophyll concentrations. Canadian Journal of Remote Sensing 21(1), 16-21.

Brown, L., Chen, J. M., Leblanc, S. G., Cihlar, J., 2000. A shortwave infrared modification to the simple ratio for lai retrieval in boreal forests: an image and model analysis. Remote Sensing of Environment 71, 16–25.

Cavayas, F., Ramos, Y., Boyer, A., 2012. Mapping urban vegetation cover using WorldView-2 imagery. Proc. SPIE 8390, Algorithms and Technologies for Multispectral, Hyperspectral, and Ultraspectral Imagery XVIII, May 8, 2012. doi:10.1117/12.918655.

Chen, J.M., 1996. Evaluation of vegetation indices and a modified simple ratio for boreal applications. Canadian Journal of Remote Sensing 22, 229-242.

Chen, J.M., Pavlic, G., Brown, L., Cihlar, J., Leblanc, S.G., White, H.P., Hall, R.J., Peddle, D.R., King, D.J., Trofymow, J.A., Swift, E., Van Der Sanden J., Pellikka, P.K.E., 2002. Derivation and validation of canada-wide coarse-resolution leaf area index maps using high-resolution satellite imagery and ground measurements. Remote Sensing of Environment 80, 165–184.

Colombo, R., Bellingeri, D., Fasolini, D., Marino, C.M., 2003. Retrieval of leaf area index in different vegetation types using high resolution satellite data. Remote Sens. Environ. 86, 120–131.

Danson, F. M., Plummer, S. E., 1995. Red-edge response to forest leaf area index. Int. J. Remote Sensing 16(1), 183-188.

DigitalGlobe, 2009. The Benefits of the 8 spectral bands of WorldView-2. http://worldview2.digitalglobe.com/docs/WorldView-2_8-Band_Applications_Whitepaper.pdf (accessed on 7/20/2011).

ENVI4.8, 2012. ITT Visual Information Solutions, Boulder, CO, www.ittvis.com.

Falkowski, M. J., Wulder, M. A., Joanne C. White, J. C., Gillis, M. D., 2009. Supporting large-area, sample-based forest inventories with very high spatial resolution satellite imagery. Progress in Physical Geography 33(3), 403–423

Fassnacht, K. S., Gower, S. T., MacKenzie, M. D., Nordheim, E. V., Lillesand, T. M., 1997, Estimating the leaf area index of north central wisconsin forests using the Landsat Thematic Mapper. Remote Sensing of Environment 61, 229-245.

Fernanades, R., Leblanc, S., Butson, C., Latifovic, R., Pavlic, G., 2002. Derivation and evaluation of coarse resolution LAI estimates over Canada. In Proceedings of Geoscience and Remote Sensing Symposium, IGARSS 02.2002, IEEE International Publication 4, 2097-2099.

Filella, I., Peñuelas, J., 1994. The red edge position and shape as indicators of plant chlorophyll content, biomass and hydric status. Int. J. Remote Sensing 15(7), 1459-1470.

FNAI and NDR (Florida Natural Areas Inventory and Department of Natural Resources), 1990. Guide to the Natural Communities of Florida, Tallahassee, Florida.

Gebreslasie, M. T., Ahmed, F. B., van Aardt, J. A. N., 2011. Extracting structural attributes from IKONOS imagery for Eucalyptus plantation forests in KwaZulu-Natal, South Africa, using image texture analysis and artificial neural networks. International Journal of Remote Sensing, 32(22), 7677-7701.

Gobron, N., Pinty, B.,Verstraete, M. M., 1997. Theoretical limits to the estimation of the leaf area index on the basis of visible and near-infrared remote sensing data," IEEE Transactions on Geoscience and Remote Sensing 35, 1438-1445.

Gómez, C., Wulder, M. A., Montes, F., Delgado, J. A., 2011. Forest structural diversity characterization in Mediterranean pines of central Spain with QuickBird-2 imagery and canonical correlation analysis. Canadian Journal of Remote Sensing 37(6), 628-642.

Gong, P., Pu, R., Miller, J. R., 1995. Coniferous forest leaf area index estimation along the Oregon transect using compact airborne spectrographic imager data. Photogrammetric Engineering & remote Sensing 61, 1107-1117.

Gong, P., Pu, R., Biging, G. S., Larrieu, M. R., 2003. Estimation of forest leaf area index using vegetation indices derived from Hyperion hyperspectral data. IEEE Transactions on Geoscience and Remote Sensing 41(6), 1355-1362.

Gong, P., R. Pu, Yu, B., 1997. Conifer species recognition: an exploratory analysis of in situ hyperspectral data. Remote Sens. Environ. 62, 189-200.

Gray, J., Song, C., 2012. Mapping leaf area index using spatial, spectral, and temporal information from multiple sensors. Remote Sensing of Environment 119 (2012) 173–183.

Gu, Z., Ju, W., Li, L., Li, D., Liu, Y., Fan, W., 2013. Using vegetation indices and texture measures to estimate vegetation fractional coverage (VFC) of planted and natural forests in Nanjing city, China. Advances in Space Research 51, 1186–1194.

Gu, Z., Ju, W., Liu, Y., Li, D., Fan, W., 2012. applicability of spectral and spatial information from IKONOS-2 imagery in retrieving leaf area index of forests in the urban area of Nanjing, China. Journal of Applied Remote Sensing 6, 063556-1-14.

Haralick, R. M., Shanmugam, K., Dinstein, I. H., 1973. Textural Features for Image Classification. IEEE Transactions on Systems, Man and Cybernetics SMC-3(6), 610–621.

Hardisky, M.A., Klemas, V. And Smart, R.M., 1983. The influence of soil salinity, growth form, and leaf moisture on the spectral radiance of Spartina alterniflora canopies. Photogrammetric Engineering and Remote Sensing 49,77–83.

Huete, A. R., 1988. A soil adjusted vegetation index (SAVI). Remote Sensing of Environment 25, 295-309.

Huete, A. R., Justice, C., van Leeuwen, W., 1999. MODIS vegetation index (MOD 13) algorithm theoretical basis document, Greenbelt: NASA Goddard Space Flight Center, http://modis.gsfc.nasa.gov/data/atbd/atbd_mod13.pdf (accessed on Nov. 10, 2014).

Huete, A.R., Jackson, R.D., Post, D.F., 1985. Spectral response of a plant canopy with different soil backgrounds. Remote Sens.Environ. 17, 37–53.

Jordan, C. F., 1969. Derivation of leaf area index from quality of light on the forest floor," Ecology 50, 663-666.

Kaufman, Y. J., Tanré, D., 1992. Atmospherically resistant vegetation index (ARVI) for EOS-MODIS. IEEE Transactions on Geoscience and Remote Sensing 30, 261–270.

Kraus, T., Schmid, M., Dech, S. W., Samimi. C., 2009. The potential of optical high resolution data for the assessment of leaf area index in East African rainforest ecosystems. International Journal of Remote Sensing 30(19), 5039–5059.

Lu, D., Batistella, M., 2005. Exploring TM image texture and its relationships with biomass estimation in Rondonia, Brazilian Amazon. Acta Amazonica 35(2), 249-257.

Munden, R., Curran, P. J., Catt, J. A., 1994. The relationship between red edge and chlorophyll concentration in Broadbalk winter wheat experiment at Rothamsted. Int. J. Remote Sensing 15(3), 705-709.

Murray, H., Lucieer, A., Williams, R., 2010. Texture-based classification of sub-Antarctic vegetation communities on Heard Island. International Journal of Applied Earth Observation and Geoinformation 12, 138–149.

Nielsen, A. A., 2002. Multiset canonical correlations analysis and multispectral, truly multitemporal remote sensing data. IEEE Transactions on Image Processing 11(3), 293-305.

Ozdemira, I., Karnielib, A., 2011. Predicting forest structural parameters using the image texture derived from WorldView-2 multispectral imagery in a dryland forest, Israel. International Journal of Applied Earth Observation and Geoinformation 13, 701–710.

Pu, R., 2012. Mapping leaf area index over a mixed natural forest area using ground-based measurements and Landsat TM imagery. International Journal of Remote Sensing 33(20), 6600–6622

Pu, R., Landry, S., 2012. A comparative analysis of high resolution IKONOS and WorldView-2 imagery for mapping urban tree species. Remote Sensing of Environment 124, 516-533.

Pu, R., Landry, S., Zhang, J., 2015. Evaluation of atmospheric correction methods in identifying urban tree species with WorldView-2 imagery. IEEE Journal of Selected Topics in Applied Earth Observations and Remote Sensing DOI: 10.1109/JSTARS.2014.2363441.

Pu, R., Gong, P., Biging, G. S., Larrieu, M. R., 2003. Extraction of red edge optical parameters from Hyperion data for estimation of forest leaf area index. IEEE Transactions on Geoscience and Remote Sensing 41(4), 916-921.

Rouse, J. W., Haas, R. H., Schell, J. A., Deering, D. W., 1973. Monitoring vegetation systems in the great plains with ERTS. in Proceedings, Third ERTS Symposium 1, 48-62.

Running, S. W., Nemani, R. R., Peterson, D. L., Band, L. E, Potts, D. F., Pierce, L. L., Spanner, M. A., 1989. Mapping regional forest evapotranspiration and photosynthesis by coupling satellite data with ecosystem simulation. Ecology 70, 1090-1101.

SAS Institute Inc., 1991. SAS/STA User's Guide, Release 6.03 Edition, Gary, NC: SAS Institute Inc., USA, 1028 pp.

Schlerf, M. T, Atzberger, C., Hill, J., 2005. Remote sensing of forest biophysical variables using Hymap imaging spectrometer data. Remote Sensing of Environment 95, 177-194.

Schmidt, A. C., 2005. A Vascular Plant Inventory and Description of the Twelve Plant Community Types Found in the University of South Florida Ecological Research Area, Hillsborough County, Florida, A thesis of the degree of Master of Science Department of Biology, University of South Florida, 1-118.

Shamsoddini, A., Trinder, J. C., Turner, R., 2013. Pine plantation structure mapping using WorldView-2 multispectral image. International Journal of Remote Sensing 34(11), 3986-4007.

Song, C., Dickinson, M. B., 2008. Extracting forest canopy structure from spatial information of high resolution optical imagery: tree crown size versus leaf area index. International Journal of Remote Sensing 29(19), 5605–5622.

Soudani, K., François, C., le Maire, G. L., Le Dantec, V., Dufrêne, E., 2006. Comparative analysis of IKONOS, SPOT, and ETM+ data for leaf area index estimation in temperate coniferous and deciduous forest stands. Remote Sensing of Environment 102, 161-175.

van Leeuwen, W.J.D., Huete, A.R., 1996. Effects of standing litter on the biophysical interpretation of plant canopies with spectral indices. Remote Sensing of Environment 55(2), 123-138.

White, J. D., Running, S. W., Nemani, R., Keane, R. E., Ryan, K. C., 1997. Measurement and remote sensing of LAI in Rocky Mountain Montane ecosystems. Canadian Journal Forest Research 27, 1714-1727.

Zhang, J., Pu, R., Yuan, L., Nie, C., Yang, G., 2014. Integrating remotely sensed and meteorological observations to forecast wheat powdery mildew at a regional scale. Journal of Selected Topics in Applied Earth Observations and Remote Sensing 7(11), 4328-4339.

Zhou, J.-J., Zhao, Z., Zhao, J., Zhao, Q., Wang, F., Wang, H., 2014. A comparison of three methods for estimating the LAI of black locust (Robinia pseudoacacia L.) plantations on the Loess Plateau, China. International Journal of Remote Sensing 35(1), 171-188.